

BraggNN: Fast X-ray Bragg Peak Analysis Using Deep Learning

Zhengchun Liu, Hemant Sharma, Jun-Sang Park, Peter Kenesei,
Jonathan Almer, Rajkumar Kettimuthu and Ian Foster
Argonne National Laboratory, Lemont, IL 60439, USA
{zhengchun.liu, hsharma}@anl.gov

May 24, 2022

Abstract

X-ray diffraction based microscopy techniques such as high energy diffraction microscopy rely on knowledge of position of diffraction peaks with high resolution. These positions are typically computed by fitting the observed intensities in detector data to a theoretical peak shape such as pseudo-Voigt. As experiments become more complex and detector technologies evolve, the computational cost of such peak shape fitting becomes the biggest hurdle to the rapid analysis required for real-time feedback for experiments. To this end, this paper proposes **BraggNN**, a machine learning-based method that can localize Bragg peak much more rapidly than conventional pseudo-Voigt peak fitting. When applied to our test dataset, **BraggNN** gives errors of less than 0.29 and 0.57 voxels, relative to conventional method, for 75% and 95% of the peaks, respectively. When applied to a real experiment dataset, a 3D reconstruction using peak positions located by **BraggNN** yields an average grain position difference of 17 μm and size difference of 1.3 μm as compared to the results obtained when the reconstruction used peaks from conventional 2D pseudo-Voigt fitting. Recent advances in deep learning method implementations and special-purpose model inference accelerators allow **BraggNN** to deliver enormous performance improvements relative to the conventional method, running, for example, more than 200 times faster than a conventional method when using a GPU card with out-of-the-box software.

1 Introduction

Advanced materials affect every aspect of our daily lives, including the generation, transmission and use of energy. Accelerating the pace of materials design promises to enhance economic activity and the transition to a cleaner energy future. However, current material design approaches rely heavily on intuition based on past experiences and empirical relationships. In order to qualify new materials for critical applications, several high-energy X-ray characterization methods have

been developed over the past decade. One of the foremost is high-energy diffraction microscopy (HEDM) [12], which provides non-destructive 3D information of structure and its evolution in the broad class of poly-crystalline materials. HEDM techniques have enabled significant breakthroughs in our understanding of processes to date through carefully designed experiments that are tractable for analysis by researchers. These methods use diffraction and tomographic imaging of up to cm-sized objects with resolutions down to the micron level.

To maximize reconstruction quality, HEDM experiments typically rotate the sample over 180° or 360° about the tomographic axis, in the process recording hundreds of diffraction peaks from each grain in the material. The reconstruction of the structure of a material using HEDM strongly relies on knowledge of the position and intensity of the diffraction signals [2, 14, 15]. Typically, a million diffraction Bragg peaks are required to reconstruct a three-dimensional structure. The position (i.e., the center of mass) of each diffraction Bragg peak needs to be located precisely and corrected for any imperfections in the detectors and artifacts in the diffraction signals.

A conventional HEDM experiment involves four steps: (1) data acquisition, (2) transfer of full scan from detector to central storage, (3) offline Bragg peak analysis to determine precise peak positions, and (4) reconstruction of grain information from the Bragg peak positions generated in the third step. Peak positions are typically computed by (optionally) transforming the peaks to polar coordinates and then fitting the peaks to a pre-selected peak shape such as Gaussian, Lorentzian, Voigt or Pseudo-Voigt. The Voigt profile, a probability distribution given by a convolution of a Cauchy-Lorentz distribution and a Gaussian distribution, is often used in analyzing data from spectroscopy or diffraction. Figure 1 demonstrate a Bragg peak and its corresponding center of mass on the Voigt profile. As one can see, the diffraction peak is not just the maxima of the photon counts; sub-pixel precision is needed to reconstruct grain characterization.

2 Motivation

It is computationally extremely expensive to fit a Voigt profile in 2D space for each Bragg peak. Significant fraction of total processing time is spent on determining peak position. Depending on sample properties and the extent of the mechanical, thermal, electromagnetic, or chemical stimulus applied to the sample, processing time can range from 10 minutes to a few weeks, even when using an HPC cluster with thousands of CPU cores. As a comparison with time on data acquisition, a single typical HEDM scan consisting of 14403600 frames takes about 615 minutes to acquire today at the Advanced Photon Source (APS) and perhaps only 50100 seconds at the planned upgraded APS (APS-U) [17] with faster detectors. Moreover, the convergence of fitting peak shape is often sensitive to model parameters, such as the choice of peak shape model and the starting point. The choice of these parameters tends to be subjective. The long data analysis time of the fresh data severely impedes measurement-based feedback for experiment steering.

Modern detectors with mega-pixel elements and frame rates that can leverage the MHz capabilities

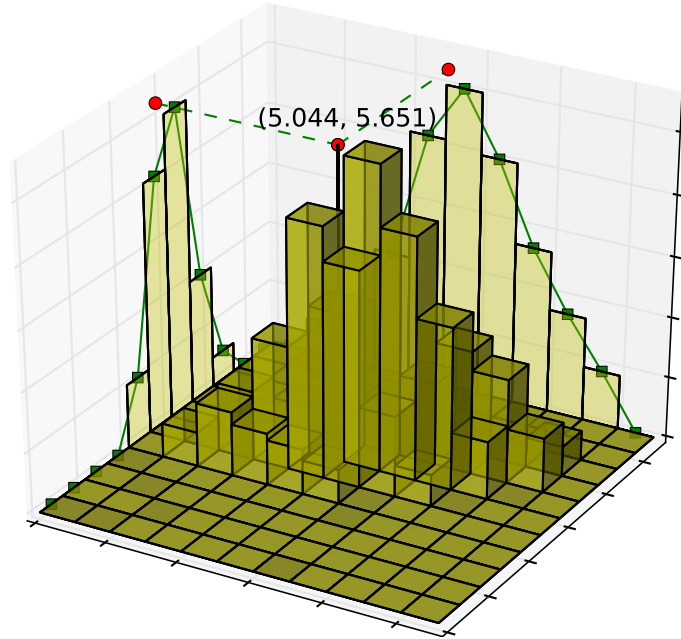


Figure 1: A diffraction peak in X-ray diffraction (11×11 patch). The height denotes photon counts, and the red dots show the peak on the Voigt profile.

of modern light sources can generate data at terabyte per second (TB/s) rates. For example, a typical HEDM measurement usually requires 4 to 16 megapixel x-ray cameras with high (12-bit) dynamic range and kHz to MHz frame rates to enable 3D in situ experiments, and thus, leads to at least $12 \text{ bits} \times (4 \text{ to } 16) \text{ Mpix} \times 1 \text{ MHz} = (6 \text{ to } 24) \text{ TB/s}$. The resulting petabyte or even exabyte datasets cannot be reasonably stored and analyzed. Thus, feature extraction must be performed at or near the detector as data are generated, to enable data reduction, experiment steering, and source and sample alignment. However, traditional algorithmic approaches such as Voigt profiling for Bragg peak analysis do not scale to maximum detector I/O capabilities without the use of a supercomputer, which is usually hard to access on-demand and requires large data transfers. A promising solution to this challenge is instead to train machine learning (ML) models, which have shown the ability to accelerate many scientific data analysis problems [10, 11], to detect specific features such as Bragg position in detector data, and deploy it in or near the detector using special-purpose deep learning model accelerator such as GPU, TPU [1] and IPU. As we show below, such models can run far much faster than conventional methods, thanks to advances in both ML methods and AI inference accelerators. It thus becomes feasible to extract peak information from streaming data in real-time, enabling rapid feedback and reducing downstream transfer, storage, and computation costs.

3 The BraggNN and its Training

In order to accelerate the Bragg peak analysis process, we form the peak localization as a machine learning problems, specifically a regression problem using supervised machine learning. We do not form it as an object localization problem because the Bragg peaks are easy to be separated from background using a heuristic threshold value, and neighbor peaks using connected-component labeling algorithm [6, 19]. Thus, the model will take a patch which contains a Bragg peak (i.e., an image) as input and directly estimate the center-of-mass of the peak. Then, we map the position of the peak in the patch back to the diffraction frame based on the location of the patch in the frame.

3.1 Model Design

Deep learning (DL) is part of a broader family of machine learning methods based on artificial neural networks to progressively extract higher level features from the pixel-level input through a hierarchical multi-layer framework. The convolutional neural network (CNN), a widely used building block of DL models for visual image analysis, is parameter efficient due to the translation-invariant property of its representations, which is the key to the success of training deep models without severe over-fitting. Although a strong theory is currently missing, much empirical evidence supports the notion that both the translation-invariant property and convolutional weight sharing (whereby the same weights are shared across an entire image) are important for good predictive performance [3].

Figure 2 shows **BraggNN**, the network architecture that we designed for locating Bragg peaks with high precision. A series of four CNN layers acting as feature extractors are followed by a series of fully connected layers that generate a regression prediction. Specifically, each CNN kernel/filter is an artificial neuron that learns (compare with traditional algorithms that kernels are hand-engineered) to extract a type of feature (e.g., various oriented edges, or blobs of color) from its input. Each 2D CNN neuron has $3 \times 3 \times c$ learn-able weights plus one learn-able bias to convolve a feature map (a 3D volume shaped as height \times width \times depth/channel) with c channels (e.g., the input patch has one channel as shown in the figure). Here we will use the first layer, which takes a Bragg peak in a patch with $11 \times 11 \times 1$ ($c = 1$) pixels as input and outputs 64 feature maps (each has 9×9 pixels), as an example to explain the convolution operation. At every convolution position, for example the one shown as dotted line in Figure 2, the dot product between the weights and the input entry ($3 \times 3 \times c$ centered at the convolution position) is computed and added by the learn-able bias. This convolution result is called activation and then it needs to pass through a rectified linear unit (ReLU, $f_{relu(x)} = \max(x, 0)$) activation function to become feature output of the layer. Each kernel is convolved (vertically and horizontally) across the input image thus results in a 9×9 feature map. Thus, although the operation is colloquially referred to as convolutions by convention, mathematically, it is a sliding dot product or cross-correlation. Each layer has multiple independent neurons that result in multiple feature maps. All feature maps are stacked along the depth dimension and then passed to the next layer as input. For example, the first layer has 64

neurons, thus it turns a $11 \times 11 \times 1$ input patch to a volume of $9 \times 9 \times 64$. Multiple convolutions layers are chained to encode the input image into a representation in latent space.

The fully connected (FC) neural network will take the encoded representation as input to estimate the center of the input Bragg peak. Similarly as the CNN layer, each FC layer has multiple artificial neurons and each neuron has a number of learn-able weights the same as its input plus one learn-able bias. The 3D feature map (e.g., $5 \times 5 \times 4$) of the last CNN layers is reshaped into a 1D vector before feeding into the first FC layer. The dot product between neuron’s weights and input is computed and added by the bias. Thus, n neurons in a given FC layer will generate an output vector of n dimension which are passed into the ReLU activation function and then serve as the input of the next layer. As one can see, different with CNN neurons that receive input from only a restricted subarea of the previous layer for each convolution point, each neuron in a FC layer is connected to all neurons in the previous layer. The output layer does not have activation function (i.e., linear activation) in our design.

The whole process that turns an input Bragg peak patch into two floating point numbers (i.e., coordination of peak center) are called feed forward pass. The ℓ_2 -norm is computed between the model output and ground truth (estimated using pseudo-Voigt profile) as the loss of the current model. Then, we compute the gradient of each neuron weights in respect to the loss function using chain rule (implemented as automatic differentiation in deep learning frameworks such as PyTorch [13]). This process to compute gradient of learn-able weights is call back propagation. The neuron’s weights are then updated using gradient descent optimization algorithm [8]. We iterate the feed-forward and back-propagation process using different pair of Bragg peak and its ground truth center many times until the model cannot make noticeable progress to minimize the ℓ_2 -norm.

The feature map size shown in the figure is an example of using a patch size of 11×11 . Depending on detector resolution, the size of the patch should be adjusted and model also needs to be retrained. In order to get a large receptive field at the early CNN layers, so as to approximate Voigt function

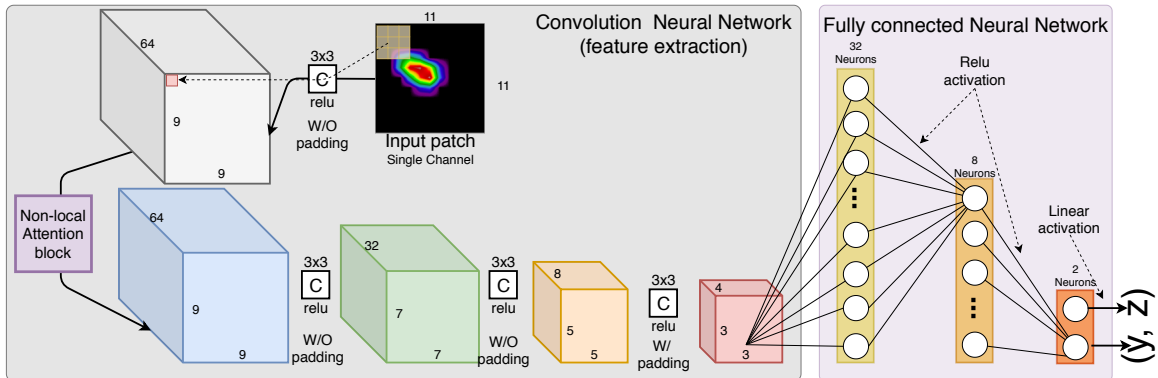


Figure 2: BraggNN deep neural network when applied to an input patch yields a peak center position (y, z) . All convolutions are 3×3 with rectifier as activation function. Each fully connected layer, except for the output layer, also has a rectifier activation function.

peaks using a global view, we place a non-local attention block [18] after the first CNN layer to extract features that capture the long-range dependencies between pixels and pay more attention to the challenging parts. An ablation study (§5.1) shows that the non-local attention block increase prediction accuracy by more than 20% on our test dataset.

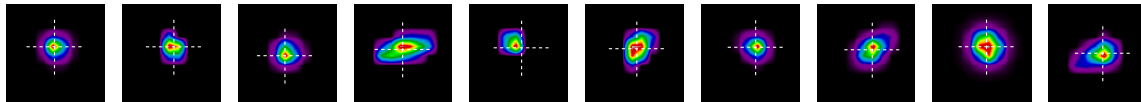
We train the **BraggNN** model with a collection of input-output pairs, each with a peak patch as input and the peak center position obtained from Voigt profiling as output. Once the **BraggNN** model is trained, we can then apply it to patches obtained from new diffraction data as follows: (1) We use the connected-component labeling algorithm [6, 19] to detect connected regions (i.e., peaks) in binary digital images. (2) For each region detected in the previous step, we determine the coordinate (row and column index of the image matrix) of its peak (maxima), and crop a patch with a pre-defined size (an odd number, must be the same as that used for **BraggNN** training) with the peak coordinate as the geometric center. Application of the trained **BraggNN** model to such a patch then yields an estimate of the peak position.

3.2 Data Augmentation

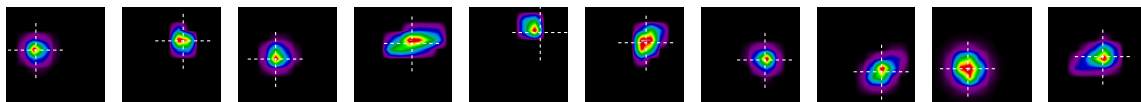
The performance of deep neural networks depends heavily on the quantity and diversity of the data used to train the model. If data are not sufficiently diverse, it is easy to experience overfitting, whereby a network learns a function with very high variance that models the training data perfectly but performs badly on other data. Many application domains, including ours, lack access to large (in terms of both quantity and diversity) and high-quality (accurately annotated) labelled data. Data augmentation is a strategy that enables practitioners to significantly increase the diversity of data available to train their DL models, without actually collecting new data. Data augmentation techniques such as cropping, padding, and flipping are commonly used to train large neural networks for image classification [4, 16] such as CIFAR-10 [9] and ImageNet [5]. While some of these existing data augmentation techniques may be useful in the Bragg peak context to avoid over-fitting, none are useful towards training a more generic model (generalize to data outside the training set for example, handle unseen peaks cropped from noisy diffraction frame) because none of the augmented samples will happen in practice.

As described in §3.1, when we use the trained **BraggNN** in practice, we prepare model inputs using the connected-component labeling algorithm which may lead to a big deviation of the actual peak center from the geometric center. This deviation do not happen in preparing training dataset because the training patches already have the peak position information and are cropped based on the actual Bragg peak center. To this end, we introduce a novel physics-inspired data augmentation method that can both avoid overfitting and help training a more generic model to deal with imperfect peak cropping from noisy diffraction frame (see §5.2). Specifically, we deviate the peak center from the geometric center randomly by a m ($m \in \mathbb{Z}$) and n ($n \in \mathbb{Z}$) pixels at horizontal (positive to right, negative to left and zero means no deviation) and vertical (positive for down, negative for up and zero for staying) direction independently, as our way of data augmentation to train the **BraggNN**

model. Thus, the data augmentation helps training a more general model because it serves as a regularization to the model. It also helps making the testing dataset statistically more similar as the peak patches for inference in practice. Figure 3 demonstrates a batch of 10 patches with (Figure 3b) and without (Figure 3a) data augmentation. Later in §5.2 we will evaluate the effectiveness of data



(a) Without data augmentation. Patches are cropped using peak center as geometric center.



(b) With data augmentation. Peaks are randomly deviated from geometric center.

Figure 3: Demonstration of a mini-batch of patches (11×11 pixels) with data augmentation for model training. As one can see, the center of mass (white cross) of some samples is intentionally drifted off ($[-2, 2]$ pixel) the geometric center in Figure 3b.

augmentation from the perspective of model generalization and prediction accuracy.

3.3 Model Training

An important tunable parameter when training a model is the input patch size, as shown in Figure 2. The patch size depends on the the voxel size of the experiment and the detector. Best practice is to choose a patch size that can fully cover all valid peaks and still leave 2–4 pixels from peak edge to patch edge for data augmentation. Since the input patch size will determine the size of neurons of the first fully connected layer, a model trained with one patch size cannot work with another patch size in practice. Another tunable parameter is for data augmentation, i.e., the interval of m and n . We typically choose the same interval size for m and n . During training, we independently sample (with replacement) a number from the interval for m and n separately in order to prepare each sample of each mini-batch online.

We implemented our model by using the PyTorch [13] machine learning framework ¹. As for dataset, we train and evaluate **BraggNN** with diffraction scan data with 1440 frames totaling 69 347 valid peaks. We used 80% of these peaks (55478) as our training set, 6000 peaks ($\sim 9\%$) as our validation set for early stopping [7], and the remaining 7869 peaks ($\sim 11\%$) as a test dataset for model evaluation, as will be discussed in §4.1. We train the model for a maximum of 80 000 iterations with a mini-batch size of 512; this takes about 1.5 hours using one NVIDIA V100 GPU. Validation-based early stopping is applied to avoid using an over-fitted model for testing and production use.

¹source code available at <https://github.com/ramsesproject/BraggNN>

4 Results Analysis and Discussion

We evaluate our model performance from two perspective: 1) distance (i.e., error) between **BraggNN** estimated center and the center using conventional Voigt profile; 2) reconstruct size and position of grains using **BraggNN** estimated peak position information, and then compare them with the reconstruction using conventional peak analysis method (e.g., pseudo-Voigt profile). We proved, from different perspective, that the grain reconstruction using **BraggNN** are non-distinguishable from which using convention methods, in relative to theoretical resolution. We then compare the computing efficiency of **BraggNN** with conventional pseudo-Voigt profile and our result also shows the computational superiority of our approach.

4.1 Model Performance

We start with quantitatively evaluating **BraggNN** by looking at the accuracy of Bragg position estimated by it. Figure 4 shows the distribution of Euclidean distance between peak centers located by the proposed **BraggNN** and the conventional pseudo-Voigt fitting. We see that the per-axis difference

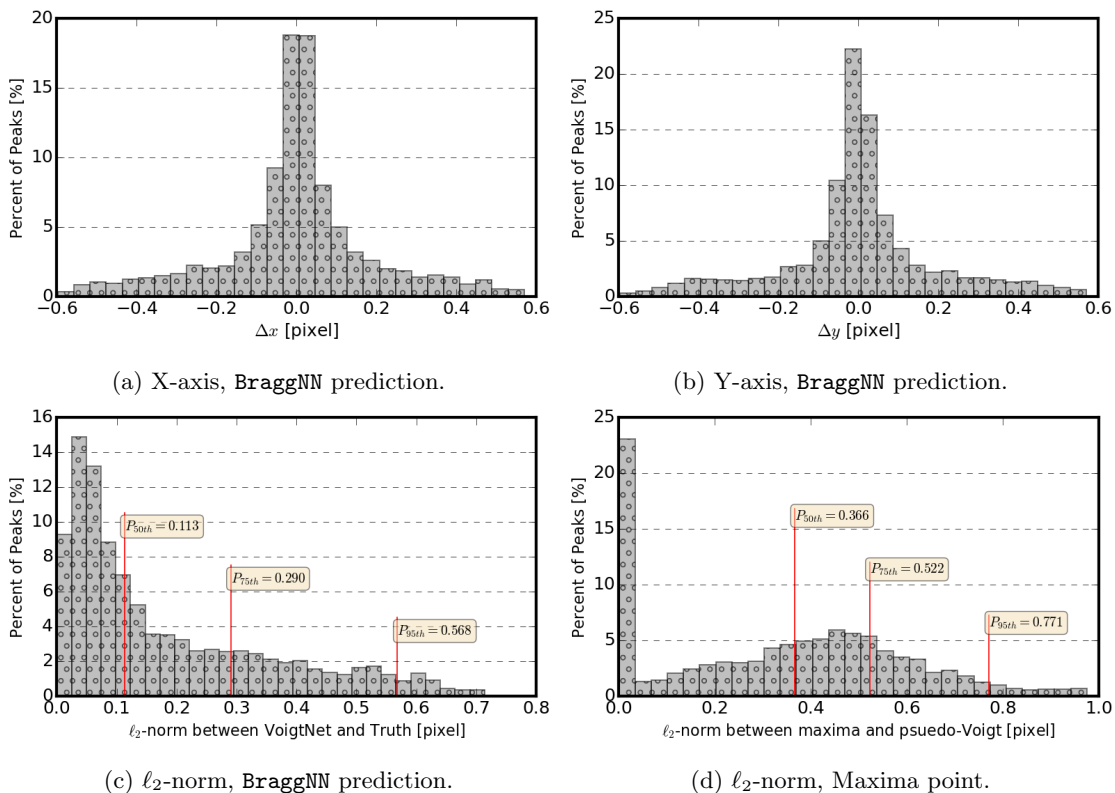


Figure 4: Distribution of difference between peak position located by **BraggNN**(a-c) or Maxima(d) and the conventional pseudo-Voigt profiling. P_{nth} in (c) and (d) denotes the ℓ_2 -norm at n_{th} percentile.

shows that the error is normally distributed around zero, which means that the model is not biased thus the error is not systematic. As quantified using Euclidean distance in Figure 4c, most peaks deviate little (e.g., 75% of peaks deviate less than 0.3 pixel) from the position identified by using the conventional Voigt profiling. In comparison, the Maxima position (has resolution of one pixel) shown in Figure 4d deviated much more than **BraggNN** from the truth (i.e., pseudo Voigt profiling).

4.2 Reconstruction Error Analysis

§4.1 discussed the direct model performance on peak localization. Since the 3D reconstruction is our final goal, we also do reconstruction using peaks position located by the proposed **BraggNN** and the conventional Voigt profiling separately. Figure 5 compares the positions of about 400 grains reconstructed separately using Bragg peaks localized by **BraggNN** and conventional 2D pseudo-Voigt profiling. The fact that the deviation directions are uniformly distributed indicates that **BraggNN** is

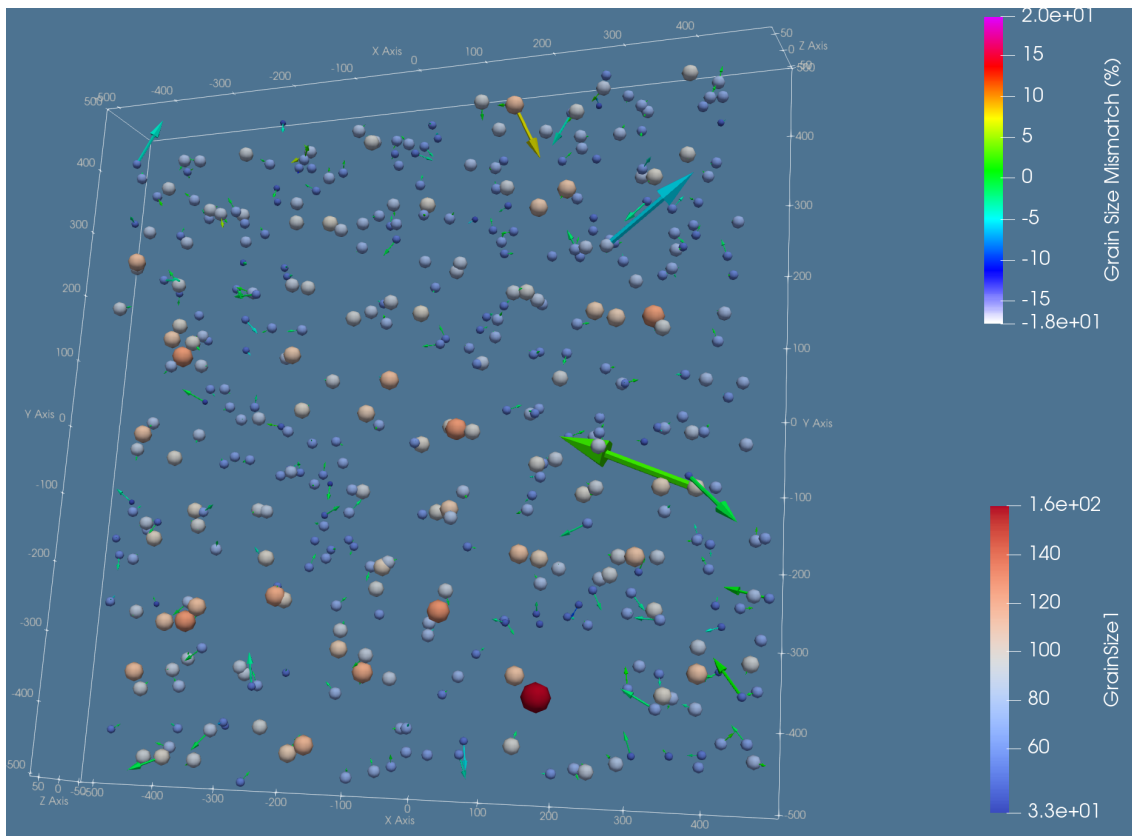


Figure 5: A comparison of grains in 3D space. Each ball represents one grain reconstructed by using the conventional method, with color indicating the grain size(μm). An arrow indicates a deviation from a grain to the corresponding grain reconstructed by using the **BraggNN** estimated peak.

not systematically biased. With the exception of a few outliers, most grains, reconstructed based on Bragg peak information using **BraggNN** or pseudo-Voigt fitting, are fully or nearly overlapped.

Figure 6 shows the Euclidean distance of the same grain reconstructed using different peaks. It is

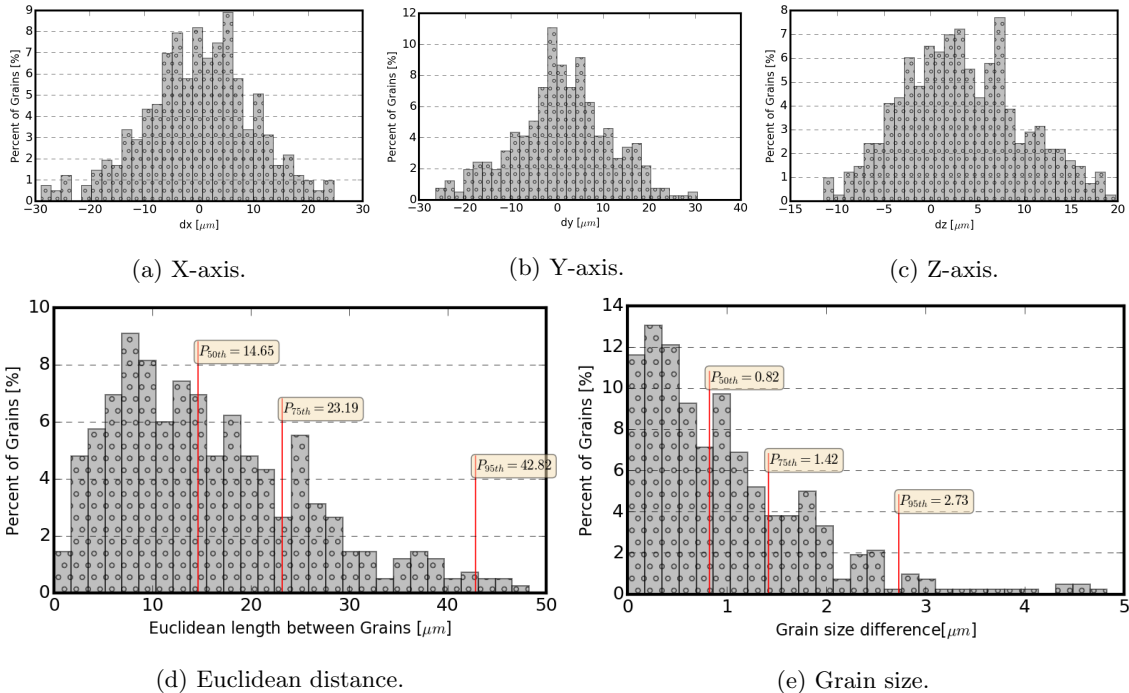


Figure 6: Distribution of difference between grains reconstructed using Bragg peak position by **BraggNN** and by the conventional Voigt profiling. P_{nth} in (d) and (e) denotes the n_{th} percentile.

clear that the distance is under acceptance limits. We note that, although we have used near-field HEDM (which provides higher resolution than the far-field HEDM reconstruction method we focused in this paper) for the same sample to verify the correctness of the peak information and the reconstructed grain information, due to the fact of ill-posed inverse problem, Bragg peaks using the conventional pseudo-Voigt is not the ground truth in theory, and there is no ground truth.

4.3 Computational Efficiency

It takes about 400 core-seconds with our C implementation of the 2D pseudo Voigt profiling to process a dataset of 800 000 peaks with an Intel Xeon E5-2630@2.6 GHz workstation CPU. On the same platform, **BraggNN** takes less than 7 core-seconds to process all peaks, a speedup of $57\times$. However, since there is no GPU-accelerated 2D pseudo Voigt fitting implementation and it is an out-of-box solution to run **BraggNN** on a GPU with any deep learning framework, we also compute the speedup by running **BraggNN** on a GPU. **BraggNN** takes only 280ms to analyze the same dataset on a NVIDIA V100 GPU, for a speedup of more than one thousand. Considering that we may not

have server-class GPU available near the experiment facility, we also evaluated **BraggNN** on a desktop with an affordable gaming NVIDIA RTX 2080 Ti GPU card, it only takes about 400ms. Thus, **BraggNN** can still offer a speedup of $250\times$ compare with running conventional Voigt profiling with a four core workstation CPU. We note that the dataset that we used for our evaluation is relatively small, having been collected at only every 0.25° . If we collect with step size of 0.01° , the conventional method will take hundreds of hours to process all peaks which **BraggNN** can do it within an hour.

5 Ablation study

We design experiments to study the effectiveness of the data augmentation method described in §3.2 and the non-local attention block in our **BraggNN** architecture design (shown in Figure 2).

5.1 Non-local Attention

We used a non-local attention block on the feature maps of the first CNN layer for **BraggNN**. The intuition behind this is that a global view at the early layer can help CNN layers better extract feature representation in the latent space for fully-connected layers to better approximate its center. Here, we conduct an ablation study to show its effectiveness. We train two models, one with attention block one without, using the same datasets, i.e., attention block is the only difference, and then we evaluate their estimation accuracy. Similar as Figure 4c, Figure 7 shows the distribution of deviations. It is clear that both 50th and 75th percentile deviation is more than 20% worse than Figure 4c where

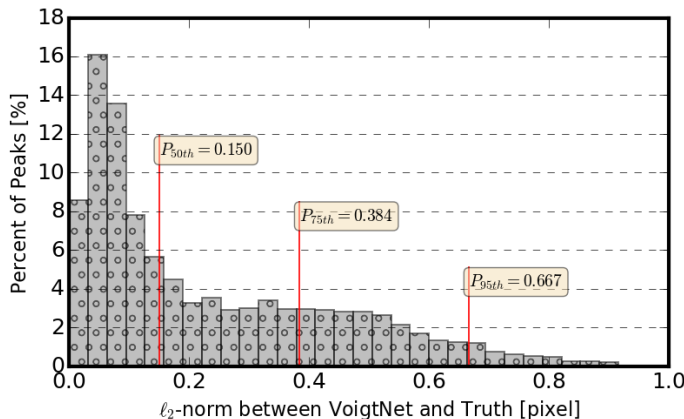


Figure 7: Distribution of difference between peak position located by **BraggNN** without the non-local attention block and the conventional pseudo-Voigt profiling.

BraggNN has the non-local attention block, the 95th percentile is about 15% worse.

5.2 Data Augmentation

We presented a novel data augmentation method in §3.2 to prevent model over-fitting and addressing inaccurate patch cropping using connect component in model inference phase. In order to study its effectiveness, we trained **BraggNN** on the same dataset with and without augmentation. When trained with augmentation, we use an interval of $[-1, 1]$ for both m and n . Figure 8 demonstrates four arbitrarily selected cases in our test dataset where peaks are deviated from their patch’s geometric center (i.e., (5, 5) for patches with 11×11 pixels) in different directions. We can see from the

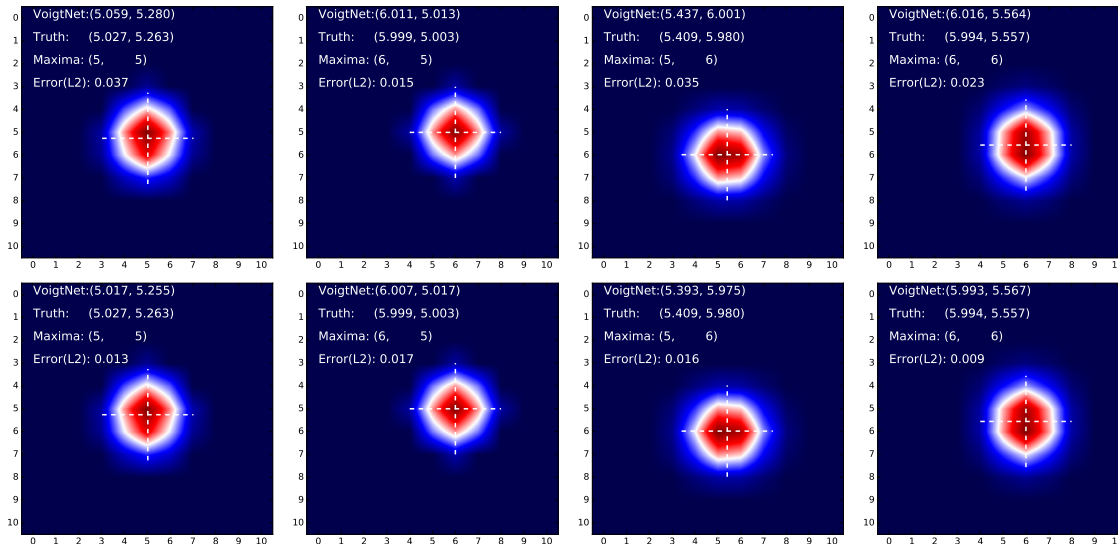


Figure 8: Peaks located by **BraggNN** when peaks is deviated from geometric center, i.e., (5, 5). The error is the Euclidean distance between truth and **BraggNN** prediction. Upper row: using **BraggNN** trained without data augmentation. Bottom row: using **BraggNN** trained with data augmentation.

demonstration that **BraggNN** is able to locate the peak values precisely even when the peak is deviated from the geometric center.

In order to quantitatively evaluate the effectiveness of data augmentation, we sample m and n independently from $\{-1, 0, 1\}$ when preparing our test dataset to mimic imperfect patch cropping. That is, only $1/3 \times 1/3 = 1/9$ of the patches have maxima at the geometric center. Figure 9 compares the prediction error on the test dataset in a statistical way. Comparing Figure 9b with Figure 9a, we see clear improvement when augmentation is applied for model training. The 50th, 75th, and 95th percentile errors are all reduced to about 20% of those obtained when **BraggNN** is trained without data augmentation: a five times improvement.

Furthermore, Figure 4c presented the distribution of ℓ_2 -norm with the same test dataset but have all the maxima position overlapped with geometric center. The **BraggNN** used was trained with data augmentation where both m and n are independently and uniformly sampled from $\{-1, 0, 1\}$. It is

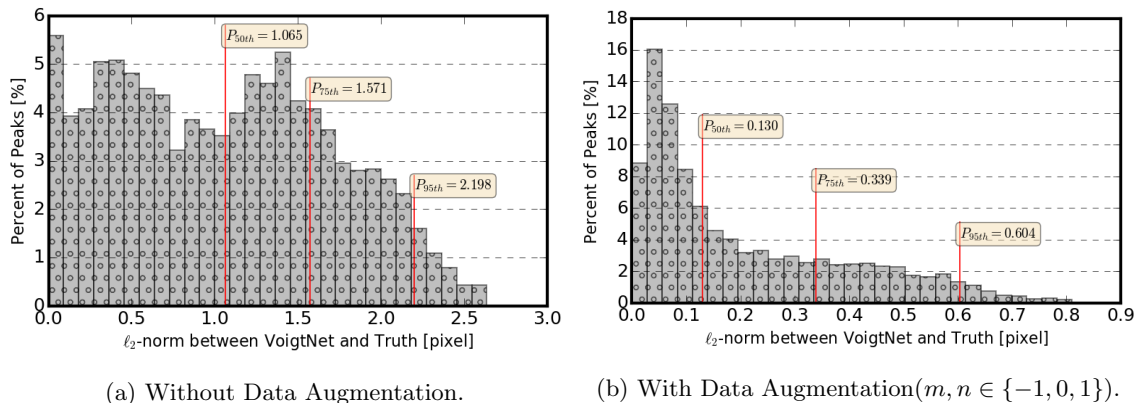


Figure 9: Distribution of difference between peak position located by **BraggNN** (with and without data augmentation) and the conventional Voigt profiling. P_{nth} in (c) denotes the n_{th} percentile.

clear that **BraggNN** trained with data augmentation can deliver similar accuracy even if 8/9 of the patches in the dataset have their maxima position deviated from the geometric center.

6 Conclusion and Future work

We have proposed **BraggNN**, the first machine learning-based method for precise locating of Bragg peaks in HEDM. When compared with conventional 2D pseudo-Voigt profiling, **BraggNN** localized peaks-based reconstruction is within acceptable deviation but can run more than $50\times$ faster on CPU and more than $250\times$ faster on a GPU without any GPU programming. The speedup enables real-time streaming analysis and experiment steering (e.g., searching area of interest for multi-scale image) that are latency sensitive.

In future work, we plan to use a deep learning-based object localization technique directly on diffraction frames to: (1) avoid labelling the connected component and, (2) deal with dense peaks diffraction where peaks are very close to each other or even partially overlapped; for which the conventional methods have an exponential complexity while the deep learning-based method has sub-linear complexity.

Acknowledgments

This material was based upon work supported by the U.S. Department of Energy, Office of Science, under contract DE-AC02-06CH11357.

References

- [1] V. Abeykoon, Z. Liu, R. Kettimuthu, G. Fox, and I. Foster. Scientific image restoration anywhere. In *2019 IEEE/ACM 1st Annual Workshop on Large-scale Experiment-in-the-Loop Computing (XLOOP)*, pages 8–13. IEEE, 2019.
- [2] A. Borbely, L. Renversade, P. Kenesei, and J. Wright. On the calibration of high-energy X-ray diffraction setups. I. Assessing tilt and spatial distortion of the area detector. *Journal of Applied Crystallography*, 47(3):1042–1053, 5 2014.
- [3] Y. Cheng, D. Wang, P. Zhou, and T. Zhang. A survey of model compression and acceleration for deep neural networks. *arXiv preprint arXiv:1710.09282*, 2017.
- [4] E. D. Cubuk, B. Zoph, D. Mané, V. Vasudevan, and Q. V. Le. AutoAugment: Learning augmentation policies from data. *CoRR*, abs/1805.09501, 2018.
- [5] J. Deng, W. Dong, R. Socher, L.-J. Li, K. Li, and L. Fei-Fei. ImageNet: A large-scale hierarchical image database. In *IEEE Conference on Computer Vision and Pattern Recognition*, pages 248–255. Ieee, 2009.
- [6] C. Fiorio and J. Gustedt. Two linear time union-find strategies for image processing. *Theoretical Computer Science*, 154(2):165–181, 1996.
- [7] I. Goodfellow, Y. Bengio, and A. Courville. *Deep Learning*. MIT press, 2016.
- [8] D. P. Kingma and J. Ba. Adam: A method for stochastic optimization. *arXiv preprint arXiv:1412.6980*, 2014.
- [9] A. Krizhevsky. Learning multiple layers of features from tiny images. Technical report, University of Toronto, 2009. <http://www.cs.toronto.edu/~kriz/learning-features-2009-TR.pdf>.
- [10] Z. Liu, T. Bicer, R. Kettimuthu, and I. Foster. Deep learning accelerated light source experiments. In *2019 IEEE/ACM Third Workshop on Deep Learning on Supercomputers (DLS)*, pages 20–28. IEEE, 2019.
- [11] Z. Liu, T. Bicer, R. Kettimuthu, D. Gursoy, F. De Carlo, and I. Foster. Tomogan: low-dose synchrotron x-ray tomography with generative adversarial networks: discussion. *JOSA A*, 37(3):422–434, 2020.
- [12] J.-S. Park, X. Zhang, P. Kenesei, S. L. Wong, M. Li, and J. Almer. Far-field high-energy diffraction microscopy: A non-destructive tool for characterizing the microstructure and micromechanical state of polycrystalline materials. *Microscopy Today*, 25(5):36–45, 2017.
- [13] A. Paszke, S. Gross, F. Massa, A. Lerer, J. Bradbury, G. Chanan, T. Killeen, Z. Lin, N. Gimelshein, L. Antiga, et al. Pytorch: An imperative style, high-performance deep learning library. In *Advances in neural information processing systems*, pages 8026–8037, 2019.

- [14] H. Sharma, R. M. Huizenga, and S. E. Offerman. A fast methodology to determine the characteristics of thousands of grains using three-dimensional X-ray diffraction. I. Overlapping diffraction peaks and parameters of the experimental setup. *Journal of Applied Crystallography*, 45(4):693–704, 8 2012.
- [15] H. Sharma, R. M. Huizenga, and S. E. Offerman. A fast methodology to determine the characteristics of thousands of grains using three-dimensional X-ray diffraction. II. Volume, centre-of-mass position, crystallographic orientation and strain state of grains. *Journal of Applied Crystallography*, 45(4):705–718, 8 2012.
- [16] C. Shorten and T. M. Khoshgoftaar. A survey on image data augmentation for deep learning. *Journal of Big Data*, 6(1):60, 2019.
- [17] S. Streiffer, S. Vogt, P. Evans, et al. Early science at the upgraded Advanced Photon Source. Technical report, Argonne National Laboratory, Oct. 2015. <https://bit.ly/2x4Vb2i>.
- [18] X. Wang, R. Girshick, A. Gupta, and K. He. Non-local neural networks. In *IEEE Conference on Computer Vision and Pattern Recognition*, pages 7794–7803, 2018.
- [19] K. Wu, E. Otoo, and A. Shoshani. Optimizing connected component labeling algorithms. In *Medical Imaging 2005: Image Processing*, volume 5747, pages 1965–1976. International Society for Optics and Photonics, 2005.

Government License

The submitted manuscript has been created by UChicago Argonne, LLC, Operator of Argonne National Laboratory (“Argonne”). Argonne, a U.S. Department of Energy Office of Science laboratory, is operated under Contract No. DE-AC02-06CH11357. The U.S. Government retains for itself, and others acting on its behalf, a paid-up nonexclusive, irrevocable worldwide license in said article to reproduce, prepare derivative works, distribute copies to the public, and perform publicly and display publicly, by or on behalf of the Government. The Department of Energy will provide public access to these results of federally sponsored research in accordance with the DOE Public Access Plan. <http://energy.gov/downloads/doe-public-access-plan>.